The nascent RNA labelling compound 5-ethynyl uridine (EU) integrates into DNA in the sea anemone *Nematostella vectensis*

Malin A. Kjosavik[1], Kathrin Garschall[1]#, Patrick R. H. Steinmetz[1]#

[1]Michael Sars Centre, University of Bergen, Thormøhlensgt. 55, N-5008 Bergen

Corresponding authors

Email addresses of corresponding authors:

Patrick R. H. Steinmetz: patrick.steinmetz@uib.no

Kathrin Garschall: Kathrin.garschall@uib.no

Keywords: Transcription, DNA replication, 5-ethynyl uridine, nascent RNA, *Nematostella*

Abstract

The detection of *de novo* synthesized mRNA transcripts is crucial for understanding the regulation of eukaryotic transcription. Using nucleoside or nucleotide analogues to label nascent RNA is complicated by the ubiquitous presence of ribonucleotide reductase enzymes (RNRs) that convert ribonucleotides into 2'-deoxyribonucleotides, the building blocks of DNA. Despite this challenge, the uridine analogue 5-ethynyl uridine (EU) has been commercialized and routinely used as specific label for nascent RNAs. Here, we employ confocal imaging, flow cytometry and biochemistry methods to demonstrate that EU integrates into RNA and at considerable levels into DNA in the sea anemone *Nematostella vectensis*. We show that inhibiting RNR by hydroxyurea abolishes cell proliferation and the incorporation of EU into DNA. Alternative compounds for labelling nascent RNA, such as 5-ethynyl cytidine (EC), 5-ethynyl uridine triphosphate (EUTP) or 2-ethynyl adenosine (EA) show similarly low specificity for integrating into RNA. Our findings indicate that ethynylated nucleosides and nucleotides, including EU, do not specifically integrate into RNA in *Nematostella*, rendering them unsuitable for visualising nascent RNAs. Based on our results and a critical review of the literature, we suggest good practice guidelines for using EU as an RNA labelling tool and discuss pitfalls and indicators that hint at unintended DNA labelling.

Summary statement

A cautionary tale about the integration of the RNA labelling compound EU (5-ethynyl uridine) into DNA in a sea anemone.

Introduction

The regulation of eukaryotic gene expression is crucial for maintaining basic cellular functions and adapting to environmental changes. In multicellular organisms (e.g., animals, plants), transcriptional regulation ensures that genes are expressed at the right time, place and levels to control embryonic development and adult homeostasis (Desvergne et al., 2006; Kaufmann et al., 2010; Levine, 2010). Intricate gene regulatory networks underlie the development and evolution of complex cell types and cellular specializations found in animals (Arendt et al., 2016; Hobert, 2008; Levine, 2010), plants (Chen et al., 2018) and some unicellular eukaryotes such as *Plasmodium sp.* (Briquet et al., 2020). A key aspect of studying gene regulation is the detection, quantification and analysis of *de novo* mRNA synthesis. As standard RNA extraction and detection procedures cannot discriminate between stored and actively transcribed mRNAs, modified nucleosides (i.e. nucleobase bound to a ribose) have been introduced in the 1960s to label and isolate nascent RNAs (Konrad, 1963; Perry, 1962; Scherrer and Darnell, 1962; Uddin et al., 1984). Before they can be integrated into RNA, nucleosides need to be tri-phosphorylated by specific nucleoside kinases to become nucleosides triphosphates (NTPs) (Voet et al., 2016). The intermediate nucleoside diphosphates (NDPs) are however not only a precursor of NTPs and RNA synthesis. Highly conserved ribonucleotide reductase (RNR) enzymes can convert NDPs into 2'-deoxy-NDPs (dNDPs) that act as precursors for DNA synthesis (Voet et al., 2016). This conserved function of RNRs to convert nucleotides into 2'-deoxynucleotides, discovered decades ago, is an essential and rate-limiting step for DNA synthesis in bacteria, eukaryotes and archaea (Greene et al., 2020; Jordan and Reichard, 1998; Nordlund and Reichard, 2006). The use of modified nucleotides therefore risks labelling not only nascent RNA but also replicating DNA. Indeed, the radioactively labelled nucleoside ^{3}H-uridine, ^{3}H-cytidine or uracil precursor ^{3}H-orotic acid, which have been developed decades ago to quantify nascent RNA synthesis via autoradiography, have been repeatedly found integrating at significant levels into DNA (Amano et al., 1965; Uddin et al., 1984). For example, the pyrimidine analogue 5-fluorouracil (5-FU) used in chemotherapy was found integrated into RNA (as 5-FU triphosphate; 5-FUTP) and DNA (as 5-fluoro-2'-deoxyuridine-5'-triphosphate; 5-

79 FdUTP) of cancer cells (Chalabi-Dchar et al., 2021; Longley et al., 2003; Major et al.,
80 1982). Similarly, the ribonucleosides cytosine arabinoside (cytarabine or Ara-C) and
81 9-β-D-arabinofuranosyl-2-fluoroadenine (F-ara-A) integrate into DNA and RNA
82 primers during DNA synthesis. This capacity, leading to the inhibition of DNA
83 replication, makes these compounds useful as chemotherapeutic agent to block
84 proliferation in rapidly dividing acute myeloid leukaemia cells (Messikommer et al.,
85 2020; Spriggs et al., 1986).

86 The recently developed nucleoside 5-ethynyl uridine (EU) uses 'click chemistry' as
87 detection method for covalently coupling fluorophores in a one-step, copper-catalysed
88 reaction. This approach avoids harsh denaturation steps necessary for
89 immunodetection and offers enhanced safety and sensitivity. EU has also been
90 claimed to specifically label RNA in mammalian cell lines (NIH 3T3), suggesting that it
91 constitutes a poor substrate for RNR (Jao and Salic, 2008). Since its introduction in
92 2008, EU has therefore been widely adopted to visualise and quantify global nascent
93 RNA synthesis and turnover in eukaryotic cells or tissues using confocal microscopy.
94 Examples include plants (Dvorackova and Fajkus, 2018) and various animals such as
95 mice (Jao and Salic, 2008), *Drosophila* (Mikhaleva et al., 2019), snails (Ierusalimsky
96 and Balaban, 2016; Ierusalimsky and Balaban, 2018) and cnidarians such as
97 *Hydractinia* (Febrimarsa et al., 2023) or *Nematostella* (Amiel et al., 2015). Many
98 studies have used EU for nascent RNA labelling without thoroughly considering a dual
99 integration into both RNA and DNA.

100 Here, we aimed to establish an EU-based assay to visualise and quantify *de novo*
101 transcriptional levels in the sea anemone *Nematostella vectensis*. It has recently been
102 shown that growth and proliferation rates of juvenile *Nematostella* polyps are strongly
103 dependent on food supply (Garschall et al., 2024). We therefore wanted to employ the
104 EU-Click system in *Nematostella* to visualise and quantify changes in nascent RNA
105 abundance upon starvation and re-feeding. We found that EU and several other
106 ethynylated nucleosides or nucleotides intensively label DNA of proliferative cells in
107 addition to RNA. This dual labelling of DNA and RNA thus renders EU unsuitable for
108 visualising and quantifying *de novo* RNA transcripts in *Nematostella*. Our results also

109 prompted us to critically evaluate the previous literature and propose guidelines to
110 prevent inadvertently identifying EU-labelled DNA as nascent RNA.

111 Results

112 EU strongly labels nuclei of proliferating cells

113 We aimed to establish Click chemistry-based EU labelling (Jao and Salic, 2008) to
114 visualise and quantify *de novo* RNA transcripts in fed juveniles of the sea anemone
115 *Nematostella vectensis* (Fig. 1A). Using flow cytometry (Supplementary Fig. 1 &
116 Methods), we benchmarked EU in different concentrations (0.5mM, 1mM and 5mM)
117 to determine the optimal working concentration. We found that 2h incubation with
118 0.5mM and 1mM resulted in similar, but small, fractions of EU-labelled cells (i.e. EU
119 index) and fluorescent signal intensities, and in a reduction of the EU index and signal
120 intensity at 5mM (Supplementary Fig. 2). As this result might indicate that higher EU
121 concentrations inhibit uptake or integration, we decided to use 0.5mM as standard
122 working concentration for EU incubation.

123 We then used confocal imaging to show that after a 2-hours long 0.5mM EU pulse
124 labelling of juvenile *Nematostella*, an unexpectedly small subset of cells exhibited high
125 EU signal (Fig. 1B-C''). Within these EU+ cells, the fluorescent signal appeared
126 broadly distributed throughout the nuclei (Fig. 1C, D-D'''), unlike the intense signal in
127 the nucleolus described from EU labelling in other systems (Bryant et al., 2022;
128 Dvorackova and Fajkus, 2018). To test if active mRNA transcription is limited to a
129 small fraction of cells in *Nematostella* juveniles, we used immunofluorescence to
130 detect phosphorylated Ser-2 (pSer2) on RNA polymerase II C-terminal repeats that
131 mark active transcription elongation. In contrast to the EU signal, however, pSer2 was
132 detected in all cells (Supplementary Fig. 3).

133 The spatial distribution and relative proportion of EU+ cells mirrored the results
134 obtained by labelling proliferative cells in fed juveniles with EdU, a 2'-deoxynucleoside
135 analogue that integrates into DNA during S-phase (Garschall et al., 2024). A direct
136 comparison showed that indeed, the EU signal strongly resembles the EdU signal after
137 a 2 hours-long incubation both in appearance and abundance (compare Fig. 1C-C''
138 with 1E-E''). As both EU and EdU contain ethynyl moieties, they cannot be

139 independently click-labelled with two different alkynylated fluorophores. We therefore
140 co-incubated EU with BrdU as alternative to EdU and found that they co-localize to
141 the nuclei of the same epidermal cells (Fig. 1F-F'''). To test if EU+ cells are indeed
142 undergoing DNA replication during S-phase, we quantified their DNA content using
143 flow cytometry (Fig. 1G, H; see Supplementary Fig. 1 and Methods for gating strategy).
144 We confirmed that the EU+ cells constitute only a small fraction (6±0.3%) of all cells
145 (Fig. 1G) and that their DNA content ranges between 2N and 4N as is typical for S-
146 phase cells (Fig. 1H). Altogether, our results thus indicate that EU consistently labels
147 the nucleus of proliferating cells in *Nematostella*.

148 **EU signal in proliferating cells is insensitive to RNase A, RNase H and the**
149 **transcriptional inhibitor actinomycin D**

150 In many organisms, DNA replication during S-phase is accompanied by mRNA
151 transcription (Wang et al., 2021). Also, DNA primase enzymes generate RNA primers
152 necessary for the initiation of DNA replication of both the lagging and leading strand
153 (Alberts et al., 2016). We therefore tested if the strong nuclear labels of EU and EdU
154 (as control) are sensitive to RNase A that degrades single-stranded RNA (Sharma et
155 al., 1993), or to RNase H that degrades RNA hybridized to DNA (Stein and Hausen,
156 1969). We found that neither RNase A nor RNase H treatments had any effect on the
157 intensity of the EU or EdU signal (Fig. 2C-F), supporting that both EU and EdU
158 integrated into DNA.

159 If EU labelled DNA, the signal should also be insensitive to RNA transcription inhibitors
160 such as actinomycin D (ActD) that inhibits RNA synthesis by intercalating into
161 transcriptionally active DNA (Goldberg et al., 1962; Sobell, 1985). ActD has previously
162 been used as inhibitor of RNA transcription to validate that EU integration into RNA is
163 transcription-dependent in cultured cells (Jao and Salic, 2008). We observed that
164 neither low (0.2μM) nor high concentrations (8μM) of ActD, applied before and during
165 a 2 hours-long EU or EdU pulse, affected the nuclear EU or EdU staining in
166 *Nematostella* (Fig. 2G-J). EU labelling of the nucleus in proliferative cells is thus
167 insensitive to transcription inhibition by ActD and to RNase A and H treatments,
168 leading us to conclude that EU integrates into DNA during S-phase.

169 Integration of EU into DNA can be explained by a multistep conversion of EU to EdU
170 that involves a reduction of the ribose to 2'-deoxyribose by the highly conserved RNR
171 enzyme. We tested this possibility by using hydroxyurea (HU), a selective inhibitor of
172 RNR which broadly arrests the cell cycle in S-phase, for example in *Hydra* (Buzgariu
173 et al., 2018; Fujisawa and David, 1982), likely by a depletion of the dNTP pool (Skoog
174 and Nordenskjold, 1971; Slater, 1973). In previous studies, this assay was used to
175 confirm that EU specifically integrates into RNA during transcription, a process that
176 should be RNR-independent (Jao and Salic, 2008; Qu et al., 2013). As expected, we
177 found that 20μM HU incubation abolishes EdU labelling (Fig. 2L) and thus blocks cell
178 proliferation. Interestingly, HU treatment in *Nematostella* also abolished EU-labelling
179 of nuclei in proliferating cells (Fig. 2K). This further confirms that EU integrates into
180 DNA of proliferating cells, possibly after being converted into EdU by RNR.

181 Finally, we tested if EU is detected in total RNA or genomic DNA of incubated animals
182 using a dot blot approach (Fig. 3A). We found that EU was detected in both the RNase
183 A-treated DNA and DNase I-treated RNA fractions (Fig. 3B, D, F, G), showing that EU
184 integrated not only into DNA, but also into RNA.

185 **EU also weakly labels RNA in small, nucleoli-like structures**

186 The finding of EU integrating into RNA led us to revisit confocal imaging of EU-labelled
187 juveniles using increased laser intensity and detector sensitivities. We indeed found
188 weak EU signal in small, punctate structures of most nuclei, potentially highlighting
189 nucleolar RNA transcription (Fig. 4A-A''). Due to the oversaturation of the fluorescent
190 signal in replicating DNA of proliferative cells, we could not determine if they contain
191 additional EU+ nucleolar puncta. The nucleolar signal was sensitive to 200μg/ml
192 RNase A treatment, while the strong label in proliferating cells remained unaffected
193 (Fig. 4B-B''). In contrast to EU, incubation with EdU did not label any nucleolus-like
194 structures, indicating that the low signal consists indeed of labelled RNA (Fig. 4C-D'').
195 Aiming to further test this assumption, we studied if the nucleolar-like label was
196 affected by inhibiting transcriptional activity with ActD (Fig. 4E, F). We observed that
197 0.2μM ActD had no detectable effect on nucleolar EU labelling (Fig. 4E). Instead, 8μM
198 ActD (Amiel et al., 2015) abolished any detectable EU+ puncti (Fig. 4F), indicating that

199 their labelling is dependent on transcriptional activity. Inhibiting RNR by using 20μM
200 hydroxyurea did not affect nucleolar EU staining, while the previously described strong
201 nuclear staining in proliferating cells was lost (Fig. 4G). Altogether, our results support
202 the conclusion that the weak, punctate EU signal corresponds to nascent ribosomal
203 RNA. The potential dual integration of EU into RNA and DNA raises the question if
204 supplementation with dNTPs could outcompete EU during DNA but not RNA
205 synthesis. Providing exogenous dNTPs in excess, however, did not result in any major
206 changes in the EU label of the nucleoli or in proliferating cells (Fig. 4H). Altogether,
207 our results suggest that EU is incorporated into both the DNA of proliferating cells and
208 the RNA of transcriptionally active cells in *Nematostella*.

209 **5-ethynyl-UTP, 5-ethynyl cytidine and 5-ethynyl adenosine are also not**
210 **specifically labelling RNA**

211 The dual labelling of DNA and RNA strongly limits the use of EU to visualise and
212 quantify *de novo* RNA transcription levels in *Nematostella*. In search for alternatives,
213 we explored the potential of 5-ethynyl-UTP (EUTP) to specifically label nascent RNA
214 in *Nematostella*, reasoning that it is likely not a direct substrate for RNR and can be
215 directly integrated into RNA (Long et al., 2022). In addition, we tested the labelling
216 characteristics of 5-ethynyl cytidine (EC) and 5-ethynyl adenosine (EA) as potential
217 alternatives. For EUTP and EC, we consistently found a strong, RNase A-insensitive
218 signal in a small subset of nuclei and a weak, RNase A-sensitive signal in small
219 nuclear puncta (Fig. 5A-D'). This strongly indicates that there are no obvious
220 differences in the labelling characteristics between EUTP, EC and EU. In contrast, EA
221 incubation led to broad, RNase A-insensitive labelling of the cytoplasm throughout the
222 epidermis (Fig. 5E, F) and especially in longitudinal and circular muscle cells (Fig.
223 5G)(Jahnel et al., 2014). Altogether, we conclude that EUTP, EC or EA are not suitable
224 alternatives to EU for the specific labelling of nascent RNA transcripts in *Nematostella*.

225 Discussion

226 Combining EU incubation with click chemistry-based fluorophore labelling promises a
227 quick, easy and commercially available method to specifically visualise nascent RNA
228 and transcriptional levels. In this study, in contrast to our expectations, we found that

229 EU considerably labelled nuclear DNA of proliferating cells in the sea anemone
230 *Nematostella vectensis*. Using confocal imaging, we showed that EU and BrdU co-
231 localized to a subset of nuclei in S-phase. In addition, we found that this strong nuclear
232 EU label in proliferative cells was not sensitive to RNase A or H. Instead, it was
233 abolished by hydroxyurea, which inhibits RNR enzymes that are essential to salvage
234 ribonucleotides for DNA synthesis (Greene et al., 2020; Jordan and Reichard, 1998;
235 Nordlund and Reichard, 2006). Biochemically, we detected EU in RNase A-treated,
236 genomic DNA extracts, further confirming that EU integrates into DNA. Together, our
237 data suggest that the strong nuclear EU label corresponds to replicated DNA strands
238 and are compatible with a scenario where RNR is part of the metabolic network
239 converting EU into EdUTP.

240 In addition, confocal imaging at higher sensitives revealed that EU labels small,
241 nucleolus-like puncta that were sensitive to RNase A treatment and to high
242 concentrations of the transcriptional inhibitor actinomycin D. The biochemical
243 detection of EU in DNase I-treated total RNA extracts confirmed integration of EU into
244 RNA. Our results strongly support that EU integrates into RNA and to a considerable
245 extent into DNA. Therefore, our study demonstrates the strong limitations of using EU-
246 click labelling to visualise and quantify nascent RNA in *Nematostella* via confocal
247 imaging, flow cytometry or fluorescence-assisted cell sorting (FACS). Likely, EU and
248 other labelled nucleosides remain useful for nascent RNA sequencing approaches,
249 such as 4sU-Seq (i.e. 4-thiouridine sequencing)(Rabani et al., 2011; Radle et al.,
250 2013) or GRO-Seq (Global Run-On Sequencing)(Core et al., 2008), as EU-labelled
251 DNA is removed during the sample and library preparation process. It should be noted
252 however that high DNA integration rates likely result in low EU-RNA labelling yields.

253 To our knowledge, EU has so far not previously been reported to label both RNA and
254 DNA in cell cultures or multicellular organisms. This is somewhat surprising as multiple
255 studies have reported a dual labelling of RNA and DNA by other labelled nucleosides
256 or nucleotides (see also introduction) (Chalabi-Dchar et al., 2021; Longley et al., 2003;
257 Major et al., 1982). Our study reinforces these doubts on the general use of labelled
258 nucleosides or nucleotides to specifically label RNA, which is often assumed but rarely
259 verified in direct and systematic ways. Strongly proliferating tissues are especially

260 prone to dual labelling as their high demands in dNTPs could increase the likelihood
261 that EU is channelled towards DNA replication and converted into EdUTP. While
262 thoroughly screening the literature, we indeed found recurring reports of EU strongly
263 labelling the whole nucleus – and not only the small nucleolar parts – in a subset of
264 cells in highly proliferative tissues. Examples of this pattern, reminiscent of DNA
265 labelling by EdU or BrdU, were found during *Nematostella* regeneration (Amiel et al.,
266 2015), in the larval zebrafish brain (Akbalik et al., 2017), the mouse intestinal crypt
267 cells (Jao and Salic, 2008; Qu et al., 2013), spermaries (Naro et al., 2017), embryonic
268 cortex (Zhang et al., 2024) and cerebellum (Van't Sant et al., 2021).

269 The specificity of RNA labelling is commonly validated by using transcriptional
270 inhibitors such as ActD (Jao and Salic, 2008; Nainar et al., 2020), or α-Amanitin
271 (Kedinger et al., 1970; Lindell et al., 1970). Previous reports show however that the
272 resulting transcriptional stress can also induce DNA damage and inhibit the cell cycle
273 (Van't Sant et al., 2021). Therefore, these inhibitors can be unreliable to validate RNA
274 specificity as the loss of EU signal after using ActD or α-Amanitin can also result from
275 inhibiting DNA replication. While ActD was effective in *Nematostella* to discriminate
276 between EU-labelled DNA and RNA label, its use might be more problematic in other
277 systems.

278 Another validation assay used to demonstrate the specificity of RNA labelling is to
279 show that the EU label is insensitive to DNase I digestion (Zocher et al., 2024). It is
280 important to note that formaldehyde-based methods used for tissue fixation leads to
281 covalent bonds between DNA and proteins (Hoffman et al., 2015). Due to these stable
282 protein-DNA complexes, treatment of EU-labelled DNA with DNase I would not
283 necessarily lead to a significant change in the signal intensity. This phenomenon is
284 observed in BrdU detection assays, where DNase I digestion is used to enhance
285 antibody accessibility without significantly compromising the BrdU signal (Tkatchenko,
286 2006).

287 The specificity of EU has been validated most extensively in *in vitro* systems (e.g. NIH
288 3T3 or HeLa cells) with the assumption that the results are transferrable to more
289 complex animal systems, such as mice (Jao and Salic, 2008; Qu et al., 2013). We

290 cannot conclusively evaluate the validity of this assumption, but our findings
291 underscore the importance of standardized controls to validate the specificity of EU or
292 other nucleotide-based RNA labelling methods in all experimentally relevant contexts.
293 Based on our experience and observations, we found that the following EU-labelling
294 characteristics are indicative of DNA integration:

295 - Broad labelling of the nucleus without clear nucleolar signal
296 - Condensed chromosome labelling in dividing cells
297 - Nuclear labelling of a smaller subset of cells in proliferative tissues
298 - Insensitivity to RNase A treatment
299 - Insensitivity to transcriptional inhibitors (e.g. ActD)

300 The occurrence of one or several of these features should prompt further validation
301 experiments. We propose the following good practice guidelines when using EU to
302 visualise nascent RNAs:

303 - **RNA specificity of EU labelling should always be validated by RNase A or**
304 **T1 treatment.** EU signal originating from the integration into RNA should be
305 sensitive to RNase A or T1 treatment. In contrast, EU-labelled DNA will not be
306 removed by RNase A or T1 treatment and may be insensitive to DNase I
307 treatment in fixed tissues (see above).
308 - **High variation of EU labelling in proliferative tissues or in cell culture**
309 **should be investigated by direct comparison with EdU or BrdU labelling.**
310 A direct comparison between cells labelled by EU and EdU or BrdU will help
311 revealing differences or similarities in labelling frequency, intensity and location.
312 We propose co-labelling of EU and BrdU on the same tissue to test if EU
313 integrates into replicating DNA of proliferative cells.
314 - **Potential cell cycle off-target effects should be considered when using**
315 **transcriptional inhibitors to control for RNA specificity.** Inhibition of
316 transcription often causes cellular stress that can alter the cell cycle, thus
317 affecting DNA synthesis rate or leading to cell death. Any resulting loss of EU
318 signal may therefore be caused by decreased transcription or blocked
319 proliferation.

320 Due to the strong limitations of EU and other RNA labelling compounds, the
321 development of new ribonucleotide analogues that more specifically label nascent
322 RNA in a wider range of organisms is necessary. Understanding the metabolic steps
323 leading to the integration of EU into DNA will help developing more specific RNA
324 labelling tools.

325 **Methods**

326 **Animal culture**

327 Adult *Nematostella vectensis* polyps derive from the original CH6 female and CH2
328 male lab strains and were cultured as previously described (Fritzenwanker and
329 Technau, 2002; Hand and Uhlinger, 1992). Shortly, adults were kept at 18°C in 16‰
330 salt concentration. The juveniles *Nematostella vectensis* polyps used in this study
331 result from crosses between wild type animals and were raised at 25°C in a darkened
332 incubator at 16‰ salt concentration (*Nematostella* medium). Polyps were fed 5x/week
333 with *Artemia* nauplii and grown until they had developed the second pair of
334 mesenteries when they were defined as 'juveniles'. The culture medium was replaced
335 on the same day after each feeding.

336 **EU, EdU, EC, EUTP or EA labelling**

337 Working concentrations for EU (5-ethynyl uridine, Invitrogen) were determined by
338 testing the fraction and fluorescent signal intensity of EU-labelled cells (EU index) by
339 flow cytometry after incubation of 0.5mM, 1mM and 5mM. As the EU index was similar
340 between 0.5mM and 1mM but reduced in the 5mM EU treatment (Supplementary Fig.
341 2A) and the fluorescent signal intensity decreased with EU concentration
342 (Supplementary Fig. 2B), all labelling experiments were carried out at 0.5mM EU.

343 *Nematostella* juveniles were prepared for incubations by relaxing them for 15 min in
344 50mM $MgCl_2$ in *Nematostella* medium. Relaxed animals were then transferred to
345 labelling medium containing 2% DMSO, 50mM $MgCl_2$ and 0.5mM EU, 0.5mM EdU (5-
346 ethynyl 2'-deoxyuridine, Invitrogen), 0.5mM EC (5-ethynyl cytidine, Jena Bioscience),
347 0.5mM EUTP (5-ethynyl UTP, Jena Bioscience) or 0.5mM EA (2-ethynyl adenosine,
348 Jena Bioscience). All incubations were carried out for 2h at RT. For unlabelled

349 controls, we used animals that were only exposed to 2% DMSO and 50mM $MgCl_2$. Up
350 to 15 animals were incubated in a single well of a 12-well plate, or up to 50 animals
351 when using a 6-well plate. Following incorporation, the animals were briefly rinsed with
352 *Nematostella* medium containing 50mM $MgCl_2$ before fixation and dissociation.

353 **Fixation and sample preparation for whole mount confocal microscopy**

354 After incubation with EU, EdU, EC, EUTP, EA and/or BrdU the relaxed polyps were
355 transferred gently into fixation solution (1x PBS, 3.7% FA, 0.2% TritonX, 0.5% DMSO),
356 incubated for 30 min at RT followed by an over-night fixation in fresh fixative at 4°C.
357 After fixation, the polyps were washed 3-5x with PTx (1x PBS, 0.2% TritonX) for
358 permeabilization, briefly blocked in PBTx (1x PBS, 0.2% TritonX, 3% BSA) and rinsed
359 with 1x PBS. The Click-iT™ reaction cocktail containing an Alexa fluorophore azide
360 (Alexa488 or Alexa555) was added to all samples, including unlabelled controls, and
361 incubated for 30 min at RT in the dark according to manufacturer protocol (Click-iT™
362 Nascent RNA/cell proliferation kit, Invitrogen). The polyps were then washed 3-5x with
363 PTx (1x PBS, 0.2% TritonX), incubated with Hoechst33342 (1:5000) and mounted for
364 confocal microscopy.

365 **Cell maceration using ACME and Click-iT™ reaction on cell suspensions**

366 For blotting of extracted DNA or RNA or to quantify the proportion and signal intensity
367 of EU cells by flow cytometry, polyps were dissociated and fixed after labelling by
368 adapting the 'ACetic acid/MEthanol' (ACME) maceration protocol to *Nematostella*
369 juveniles as previously described (García-Castro et al., 2021; Garschall et al., 2024).
370 Shortly, 5ml of fresh ACME solution (15% methanol/10% glacial acetic acid/10%
371 glycerol in Milli-Q water) were added to labelled polyps in gentleMACS™ C-tubes
372 (Miltenyi Biotec). During the ACME incubation, all tubes were kept on a see-saw
373 shaker. Dissociation using the gentleMACS™ tissue homogenizer (Miltenyi Biotec)
374 was started after 10 min by running the program “B_01” for initial dissociation, followed
375 by four runs of the “Multi_A_01” programme over the following 50 min until all tissue
376 was dissociated. The resulting cell suspension was washed twice with 10ml of ice-cold
377 1×PBS/1% BSA, pelleted for 5min at 800*g* at 4°C, resuspended in 1ml of 1× PBS/1%
378 BSA and filtered through a pre-wetted 50μm CellTrics strainer (Sysmex). The resulting

379 cells were permeabilized with PTx (1x PBS, 0.2% TritonX) at RT for 15 min, washed
380 with 1x PBS and incubated for 30 min at RT in the dark with a modified Click reaction
381 cocktail (Click-iT™ Nascent RNA kit, Invitrogen) where the reaction buffer was
382 replaced by 1x PBS. The cells were then pelleted in a centrifuge by spinning for 5min
383 at 800*g* at 4°C. Cells were then washed with PTx and transferred to 1xPBS containing
384 1% BSA for short term storage at 4°C or to 90% Methanol long-term storage at -20°C.

385 **EU/BrdU co-labelling assay and RNA Pol II-Ser2 immunofluorescence**

386 The EU/EdU co-labelling mix was prepared by combining 100*µ*M BrdU (5-Bromo-2´-
387 deoxyuridine, Invitrogen) and 500*µ*M EU in *Nematostella* medium with 2% DMSO and
388 50mM $MgCl_2$. After 2h of incubation, animals were rinsed with *Nematostella* medium
389 containing 50mM $MgCl_2$, followed by fixation and the Click-iT™ reaction to Alexa
390 Fluor™ 555 (Invitrogen) as mentioned above.

391 To make the DNA accessible for BrdU immunostaining, the tissue was incubated with
392 2M HCl in 1xPBS for 30 min at RT, followed by multiple washes with PBTx (1x PBS,
393 3% BSA, 0.2% TritonX) and a blocking step for 2h at RT in blocking solution (5% NGS,
394 3% BSA and 0.02% TritonX in 1x PBS). The primary anti-BrdU rabbit antibody 1:500
395 (Invitrogen, PA5-32256) was diluted in blocking solution and incubated o/n at 4°C on
396 a rotation shaker without inversion. After 3 washes with PBTx, the tissue was blocked
397 for 1h at RT in freshly prepared blocking solution and incubated for 2h at RT with
398 1:1000 goat-anti-rabbit-Alexa488 antibody (Invitrogen, A-11034), 1:5000
399 Hoechst33342 (Life Technologies) in blocking solution. Samples were then washed 3
400 times in PTx to reduce unspecific signal.

401 For the immunofluorescence labelling of RNA Pol II CTD repeat YSPTSPS phospho-
402 Ser2 (AB5095, Abcam), indicative of active transcription, polyps were fixed after 2h
403 EU incorporation o/n at 4°C, washed and blocked for 1h in blocking solution (5% NGS,
404 3% BSA and 0.02% TritonX in 1x PBS). Primary antibody (AB5095, Abcam) was
405 diluted 1:500 in blocking solution and incubated at 4°C over night on a rotation shaker
406 without inversion. Samples were washed 5 times with PBTx (1x PBS, 3% BSA, 0.2%
407 TritonX) and blocked for 30 min in blocking solution at RT. Secondary goat-anti-rabbit-
408 Alexa488 antibody (Invitrogen, A-11034) was added 1:1000 along with 1:5000

409 Hoechst33342 and incubated for 2 h at RT. Samples were then washed 3 times and
410 mounted for confocal microscopy.

411 **Confocal imaging**

412 Images of whole mount polyps were taken using juvenile polyps that were cut
413 transversally using a razorblade, and mid-section pieces were mounted on slides
414 using ProLong Gold™ (Invitrogen). Confocal imaging was performed using an
415 Olympus FLUOVIEW FV3000 confocal microscope with standard PMT detectors and
416 a 60x silicon-immersion lens. All epidermal images were recorded as z-stacks using
417 laser power and sensor sensitivity settings that were kept identical between
418 acquisitions within each of these groups of images: (i) strong nuclear EU label in
419 proliferating cells (Fig. 2A, C, E, G, I, K); (iia) nucleolar EU/EdU label (Fig. 4A-D'') or
420 (iib) Fig. 4E-H; (iii) EdU label (Fig. 2B, D, F, H, J, L); (iv) EUTP nuclear label (Fig. 5A-
421 B); (v) EUTP nucleolar label (Fig. 5A'-B'); (vi) EC nuclear label (Fig. 5C-D); (vii) EC
422 nucleolar label (Fig. 5C'-D'); (viii) EA label (Fig. 5E-F). Images were consistently
423 adjusted for brightness and contrast over all images within each group of images using
424 the QuickFigures PlugIn (Mazo, 2021) in Fiji/ImageJ (Schindelin et al., 2012;
425 Schindelin et al., 2015), except for the DNA stain that has been adjusted differently
426 between images.

427 **Flow cytometry**

428 For each of the experimental conditions (0.5mM, 1mM or 5mM EU), 2 (2% DMSO
429 control) or 3 (all others) replicate pools of 7 juveniles each were dissociated and fixed
430 using ACME and coupled to Alexa Fluor™ 555 as described above. The cell
431 suspensions were stained with 1μg/ml FxCycle violet DNA dye (Invitrogen) at 4°C
432 over-night and run on an LSRFortessa™ (BD Life Sciences) flow cytometer. EU-
433 labelled cells were analysed using FlowJo version 10.8 (BD Life Sciences) (see gating
434 strategy Supplementary Fig. S1). Shortly, individual cells were gated using FSC and
435 SSC parameters before selecting for cells with a FxCycle violet DNA signal ranging
436 between 2N and 4N. Within this cell population, cells were considered EU positive if
437 their Alexa555 signal was above the threshold of the unlabelled, 2% DMSO samples.

438 Individual cells were visualised after flow cytometry by adding 2 µg/ml Concanavalin
439 A conjugated to Alexa Fluor™ 488 to label cytosol in EU-labelled cell suspensions.

440 **Flow cytometry data analysis**

441 The fraction of EU positive cells in flow cytometry as well as their fluorescent intensity
442 were analysed between different concentration of EU (0.5mM/1mM/5mM) using One-
443 way ANOVA. Pairwise comparisons between the different EU concentrations were
444 calculated in Tukey's multiple comparison test and adjusted p-values indicated as
445 asterisks (Supplementary Figure 2).

446 **Hydroxyurea, actinomycin D and dNTPs incubations**

447 Juveniles were pre-incubated for 30 min with 20μM hydroxyurea (Sigma, H8627),
448 0.2μM or 8μM actinomycin D (Invitrogen, A7592) in 1% DMSO and 50mM $MgCl_2$ in
449 *Nematostella* medium prior to adding EU, EdU or DMSO to reach a final concentration
450 of 0.5mM EU or EdU and 2% DMSO. Animals were incubated for 2 hours. dNTPs
451 (New England Biolabs) were added directly into the EU labelling medium for a 2h
452 incubation at a final concentration of 2mM (0.5mM per nucleotide) in 2% DMSO.

453 **Incubation in RNase A or RNase H**

454 Following the Click reaction, the samples were treated with 200μg/ml RNase A
455 (PureLink™, Invitrogen) in PTx (0.2% TritonX, 1x PBS) for 15 min at 37°C, or 100U/ml
456 RNase H (Thermo Fisher Scientific) in 1x RNase H Reaction Buffer for 30 min at 37°C,
457 followed by 3-5 washes with PTx before mounting and confocal microscopy.

458 **Total RNA extraction for visualising on a dot blot**

459 Per sample, 50 EU-labelled animals were homogenized in 10ml of ACME solution with
460 all washing steps described above unchanged but without filtering through CellTrics™
461 strainers. After the Click reaction to Alexa Fluor™ 488, half of the resulting cell pellet
462 was used for total RNA and half for genomic DNA extraction.

463 For total RNA extraction, the cells were mixed with 1ml of TRIzol reagent (Invitrogen)
464 and stored at -20°C for up to a week. Total RNA extraction was done by adapting the
465 manufacturer's protocol. Shortly, samples were brought to RT for 5min before mixing
466 the pellets with 200μl 100% chloroform. Samples were gently mixed for 3 min by

467 repeated inversion and centrifuged at full speed (16.000 g) at 4°C. The aqueous phase
468 was transferred to a new tube and, after addition of an equal volume of 100%
469 isopropanol, shortly mixed by inversion and incubated for 15 min at RT. RNA was
470 pelleted by centrifuging for 15min at full speed (16 000 g, 4°C). Pellets were washed
471 with freshly prepared 80% ethanol and centrifuged again for 15min at full speed
472 (16 000 g) at 4°C. All ethanol was carefully removed and dried off on a heated block
473 at 60°C. RNA was resuspended in 10μl of ultrapure water and digested with 2U
474 TurboDNase (Invitrogen) in 30μl for 30min at 37°C according to manufacturer's
475 protocol. RNA precipitation was done at 2.5M LiCl (from MEGAscript® T3 kit,
476 Invitrogen) and 20 μg of glycogen (Roche) at -20°C for 30 min. RNA was pelleted by
477 centrifuging for 15min at full speed (16 000 g, 4°C) and washed with ice cold 80%
478 Ethanol. After air-drying the pellet, RNA was resuspended in ultra-pure water and
479 concentration was measured on a NanoDrop (Thermo Scientific).

480 **Genomic DNA extraction**

481 After ACME dissociation and Click reaction, cell suspensions of labelled and control
482 animals were stored in TE Buffer (10mM Tris pH 8, 1mM EDTA pH 8, 25mM NaCl) at
483 -20°C for up to a week. After thawing, 100μg/ml Proteinase K was added and the cells
484 were incubated at 50°C until fully digested (15-20 min). Each sample was mixed with
485 1ml of phenol by inverting and centrifuged for 3 min at full speed (16 000 g) at RT. The
486 supernatant was transferred to a fresh tube and 1ml of phenol/chloroform (1:1 mix)
487 was added and the mix was centrifuged for 3 min at full speed. The supernatant was
488 mixed with 1ml of 100% chloroform and spun down for 3 min at full speed. Again, the
489 supernatant was transferred to a new tube and precipitated with 100 μl 3M Na-Acetate
490 pH 5.2 and 1ml of ice-cold 100% ethanol. DNA was pelleted by centrifugation for 10
491 min at full speed (16 000 g, 4°C), washed with ice-cold 70% ethanol and spun down
492 again. After the ethanol was removed, the pellet was air-dried and resuspended in TE
493 buffer. The DNA was then incubated with 100μg/ml RNase A for 15 min at 37°C and
494 precipitated again using 0.1 vols 3M Na-Acetate and 2.5 volumes of ice-cold 100%
495 ethanol. DNA was pelleted by 10 min centrifugation at full speed (16 000 g, 4°C) and
496 washed with 80% ice-cold ethanol. After removal of ethanol and air-drying, the DNA

497 pellet was taken up into ultra-pure water and its concentration was measured on a
498 NanoDrop (Thermo Scientific).

499 **Typhoon imaging**

500 ACME fixed cell suspensions of EU-labelled animals and controls were split after
501 coupling to Alexa Fluor™ 488 for genomic DNA and total RNA extractions (see above).
502 0.4 μg of total RNA and genomic DNA were blotted on an Amersham Hybond™ -N$^+$
503 membrane and the Alexa488 fluorescence was read with a Typhoon biomolecular
504 imager (FLA 9000) using a 473 nm laser with the standard LPB filter.

505

Acknowledgements

We thank Simon Henriet for support and materials for the membrane blotting experiment, Eudald Pascual-Carreras, Jørn Skavland and Brith Bergum for help and support with flow cytometry, Andreas Midlang for help with confocal imaging, Eilen Myrvold and Brandon Mellin for help with *Nematostella* husbandry, and the whole S12 lab for critical discussion. The flow cytometry was performed at the Flow & Mass Cytometry Core Facility, Department of Clinical Science, University of Bergen. The confocal imaging was performed at the Michael Sars Centre and the BIO Department at UiB.

Competing interests

The authors declare no competing interests.

Funding

P.R.H.S. and K.G. received funding from the Research Council of Norway (234817 and 335230).

521 **Figures**

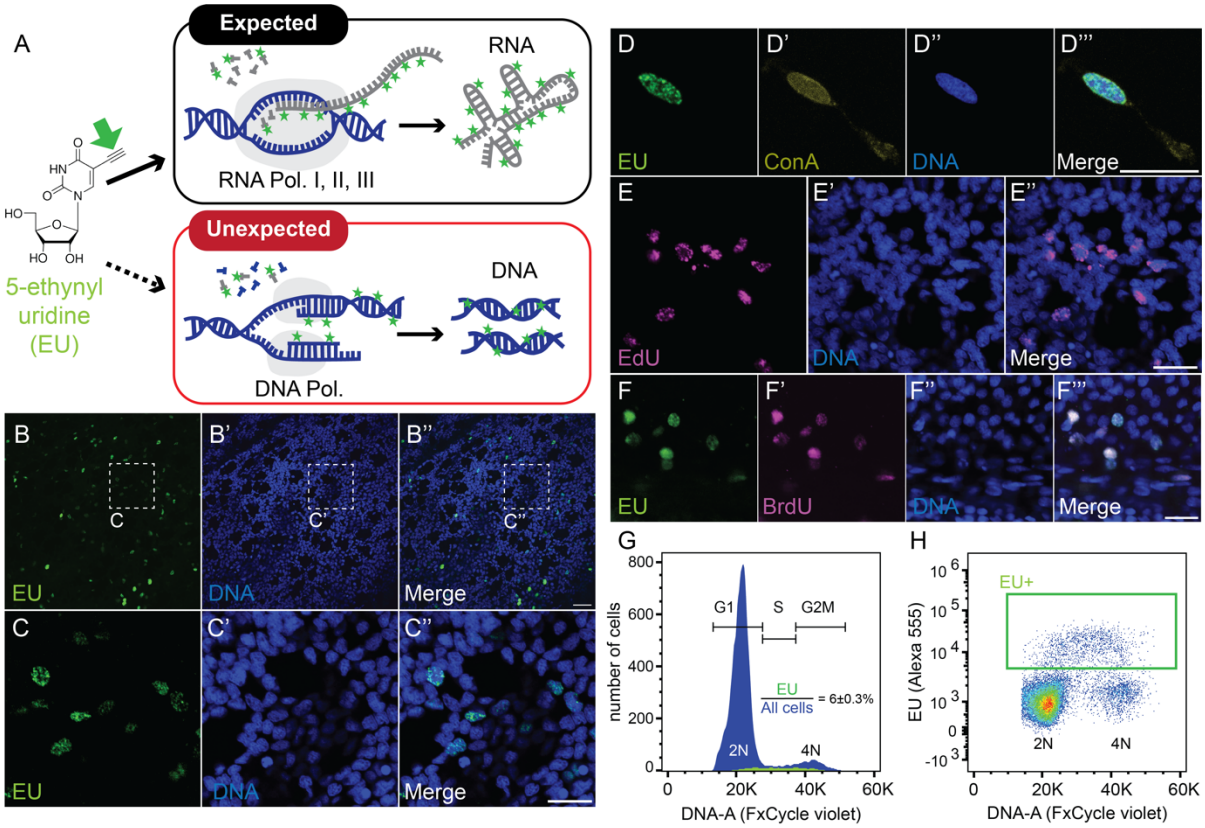

522 **Fig. 1. EU labels the nucleus of proliferating cells. (A)** Schematic overview of EU
523 integration into RNA by RNA polymerases, or alternatively into replicating DNA by
524 DNA polymerases during the S-phase of the cell cycle. Green arrow highlights the
525 ethynyl moiety used to couple a fluorophore by click chemistry. Green stars represent
526 fluorophores. **(B-F''')** Single confocal images of epidermal cells labelled for EU (B-D'''),
527 EdU (E-E'') or co-labelled for EU and BrdU (F-F''') in juvenile *Nematostella* sea
528 anemones. C-C'' represent higher magnification of the areas labelled in B-B''. D-D'''
529 represent high magnifications of a labelled nucleus to show nuclear morphology. Note
530 the absence of any labelled nucleolus-like structures. **(G-H)** Flow cytometry histogram
531 of FxCycle Violet DNA stain (G) or Density plot of DNA dye (DNA-A) and EU signal
532 intensity (Alexa555) (H) show that EU+ cells range between 2N and 4N DNA content.
533 G1, S and G2M: typical DNA content of cell cycle phases. Colour gradient in (H)
534 represents event density from high (red) to low (blue). ±: represents standard error of
535 the mean. Flow cytometry: n=3 replicates. Nuclear stain (blue in B'-C'' and E'-F''):
536 Hoechst33342. ConA: Concanavalin A. K: 1.000; Pol. Polymerase. Scale bars: 20μm
537 (B'') or 10μm (C'', D'', E'', F''').

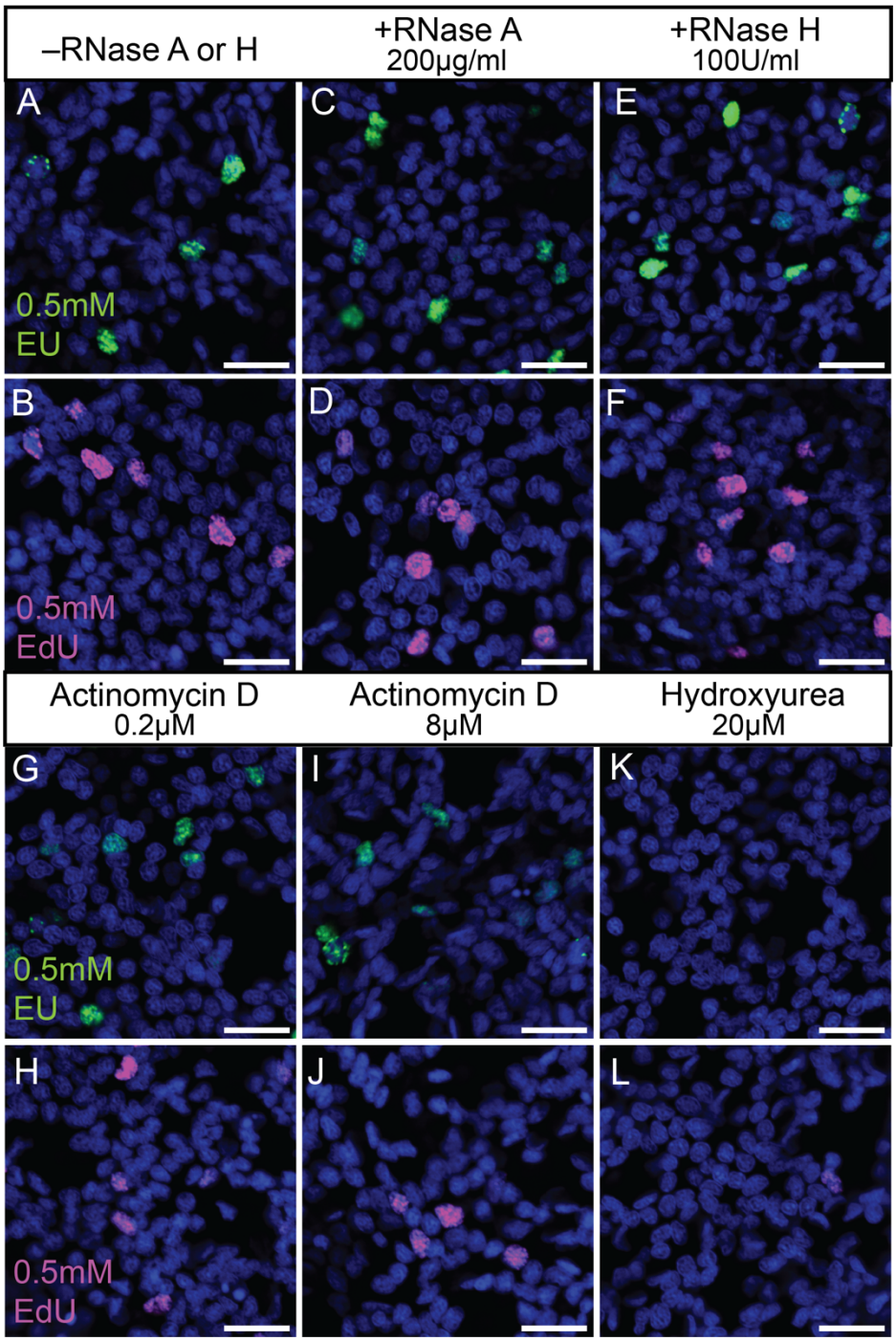

Fig. 2. Nuclear EU label in proliferating cells is insensitive to RNase A, RNase H and actinomycin D, but sensitive to hydroxyurea. (A-L) Single confocal images of epidermal cells labelled for EU (A, C, E, G, I, K) or EdU (B, D, F, H, J, L) in juvenile *Nematostella* sea anemones without any treatment (A, B), or treated with RNase A (C, D), RNase H (E, F), the transcriptional inhibitor ActD at 0.2μM (G, H) and 8μM (I, J), or the ribonucleotide reductase (RNR) inhibitor hydroxyurea (K, L). Nuclear stain (blue): Hoechst33342. Scale bars: 10μm.

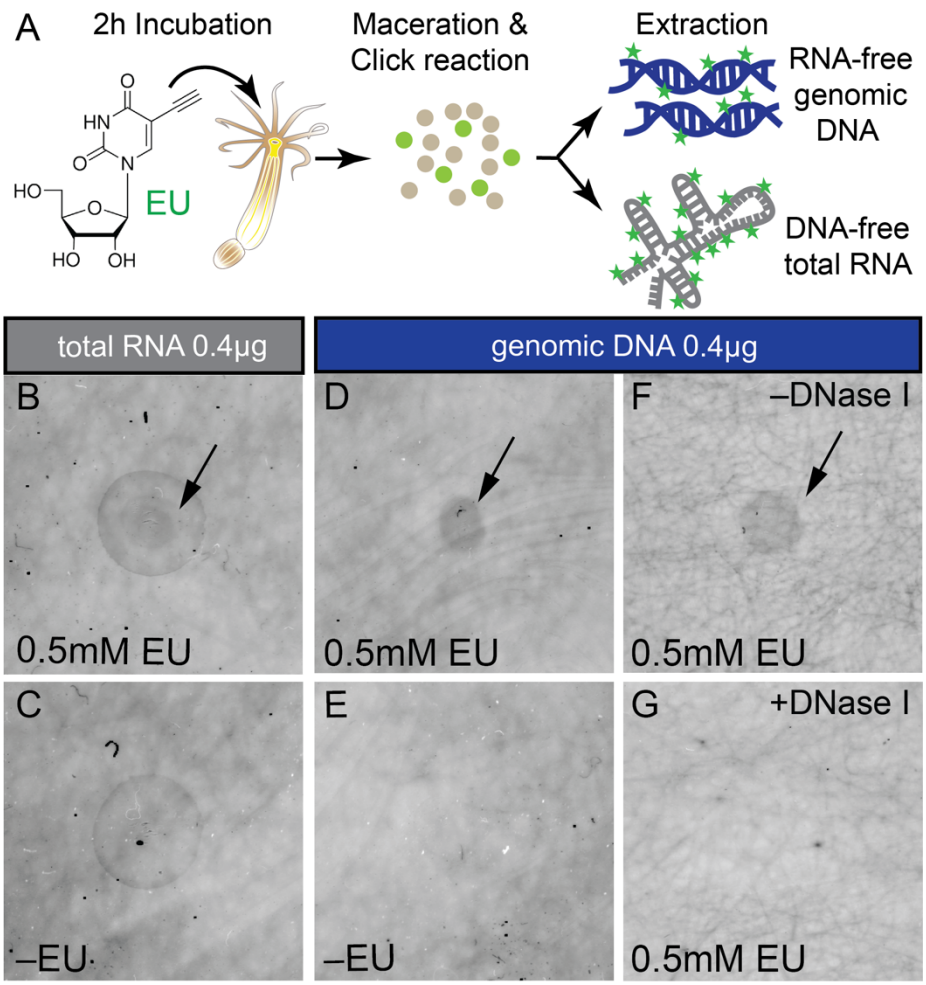

Fig. 3. EU is detected in extracted genomic DNA and total RNA. (A) Schematic summary of experimental setup. See Methods for details. **(B-G)** Dot blots of DNA-free total RNA (B, C) or RNA-free genomic DNA (D-G) from animals incubated with (B, D, F, G) or without EU (C, E), and treated without (F) or with DNase I (G). Sample volume put on blot corresponded to between 2 and 10μl.

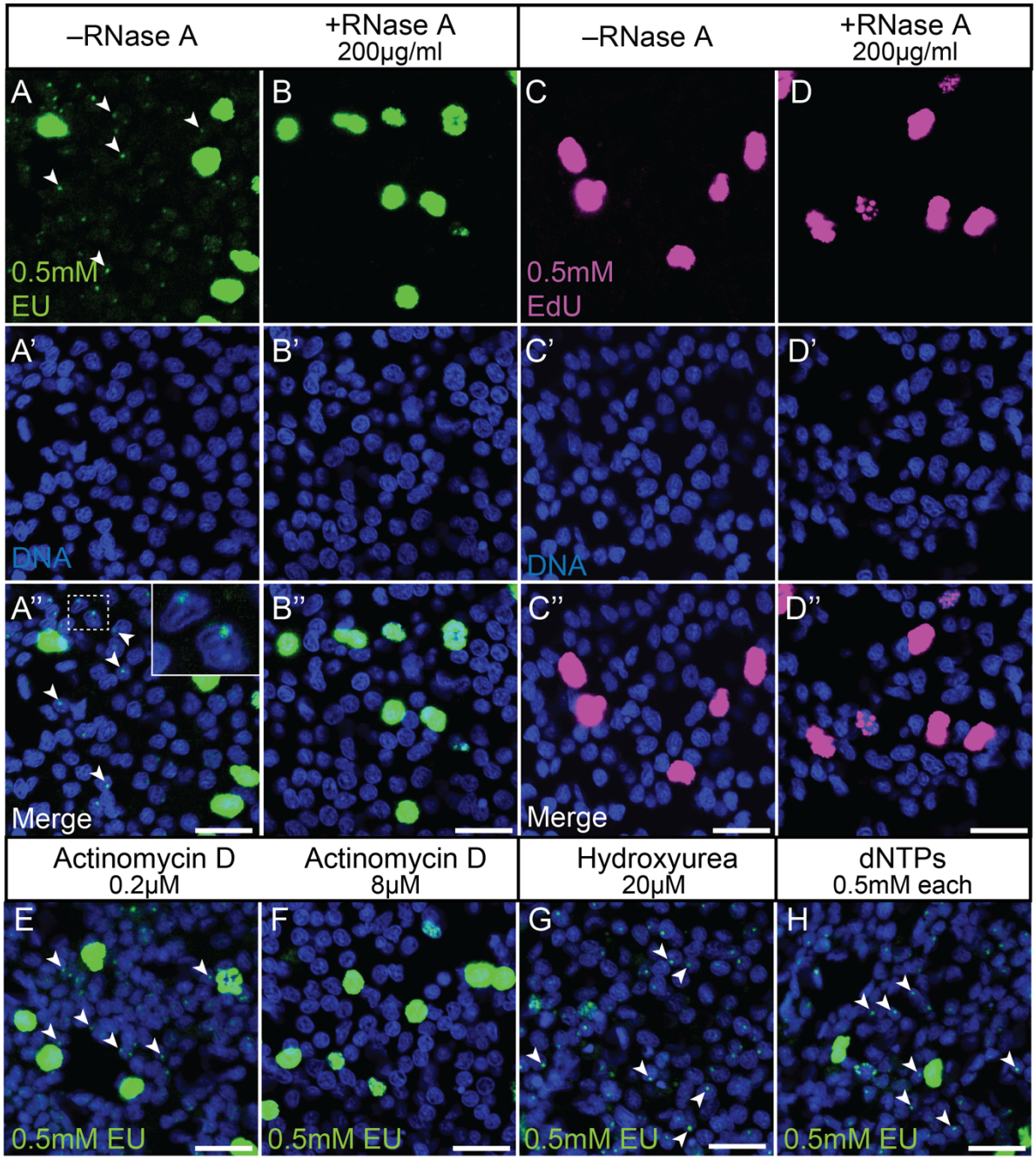

Fig. 4. Small, nucleolus-like dots after EU but not EdU labelling are sensitive to RNase A and actinomycin D, but insensitive to hydroxyurea or an excess of dNTPs. Single confocal images of epidermal cells labelled by EU (A-B", E-H) or EdU (C-D") and acquired at relatively high laser intensities and detector sensitivities. **(A-B")** EU labels small, nucleolus-like dots (arrowheads) that are lost after RNase A treatment. Inlet in A" shows higher magnification of the boxed area and depicts labelled nucleolus-like dots in two nuclei. **(C-D")** Using the same detection parameters as in A-B", EdU label is specific to nuclei of proliferating cells (C-D"). **(E-F)** EU label in

558 small nucleolus-like dots (arrowheads) is insensitive to low (E) but abolished by high
559 concentrations (F) of the transcriptional inhibitor ActD. **(G)** Inhibition of ribonucleotide
560 reductase by hydroxyurea leads to reduction of strong nuclear staining, but not of the
561 small nucleolus-like label (arrowheads). **(H)** Adding an excess of dNTPs appears to
562 have no effect on the EU label. Nuclear stain (blue): Hoechst33342. Scale bars: 10μm.

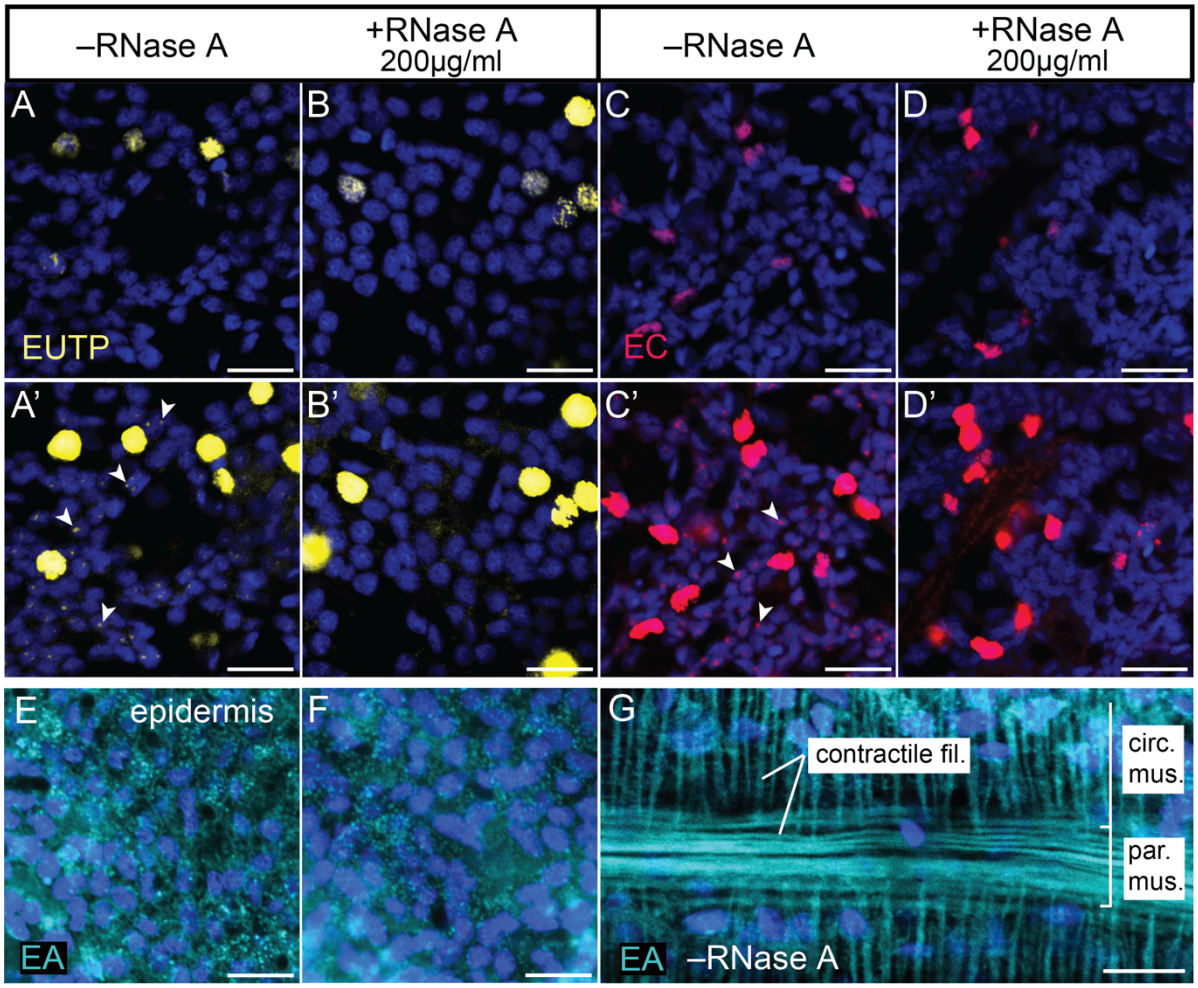

563 **Fig. 5. The potential EU alternatives 5-ethynyl uridine triphosphate (EUTP), 5-**
564 **ethynyl cytidine (EC) and 2-ethynyl adenosine (EA) also integrate in non-RNA**
565 **structures.** Single confocal images (A-F) or confocal imaging stacks (G) of epidermal
566 (A-F) or gastrodermal (G) cells labelled using EUTP (yellow), EC (red) or EA (cyan).
567 **(A-D')** EUTP (A-B') and EC (C-D') are detected in dispersed nuclei of putative
568 proliferating cells and their signal is RNase A-insensitive (A-D). At high laser intensity
569 and detector sensitivity, both compounds also label small nucleolus-like dots
570 (arrowheads) that are RNase A-sensitive (A'-D'). **(E-G)** EA label is found broadly in
571 epidermis (E) and is insensitive to RNase A degradation (F). EA signal is also
572 prominently found in contractile filaments of muscle cells (G). Nuclear stain (blue):
573 Hoechst33342. circ. mus.: circular muscle; fil.: filaments; par. mus.: parietal muscle.
574 Scale bars: 10μm.

575 **Supplementary Figures**

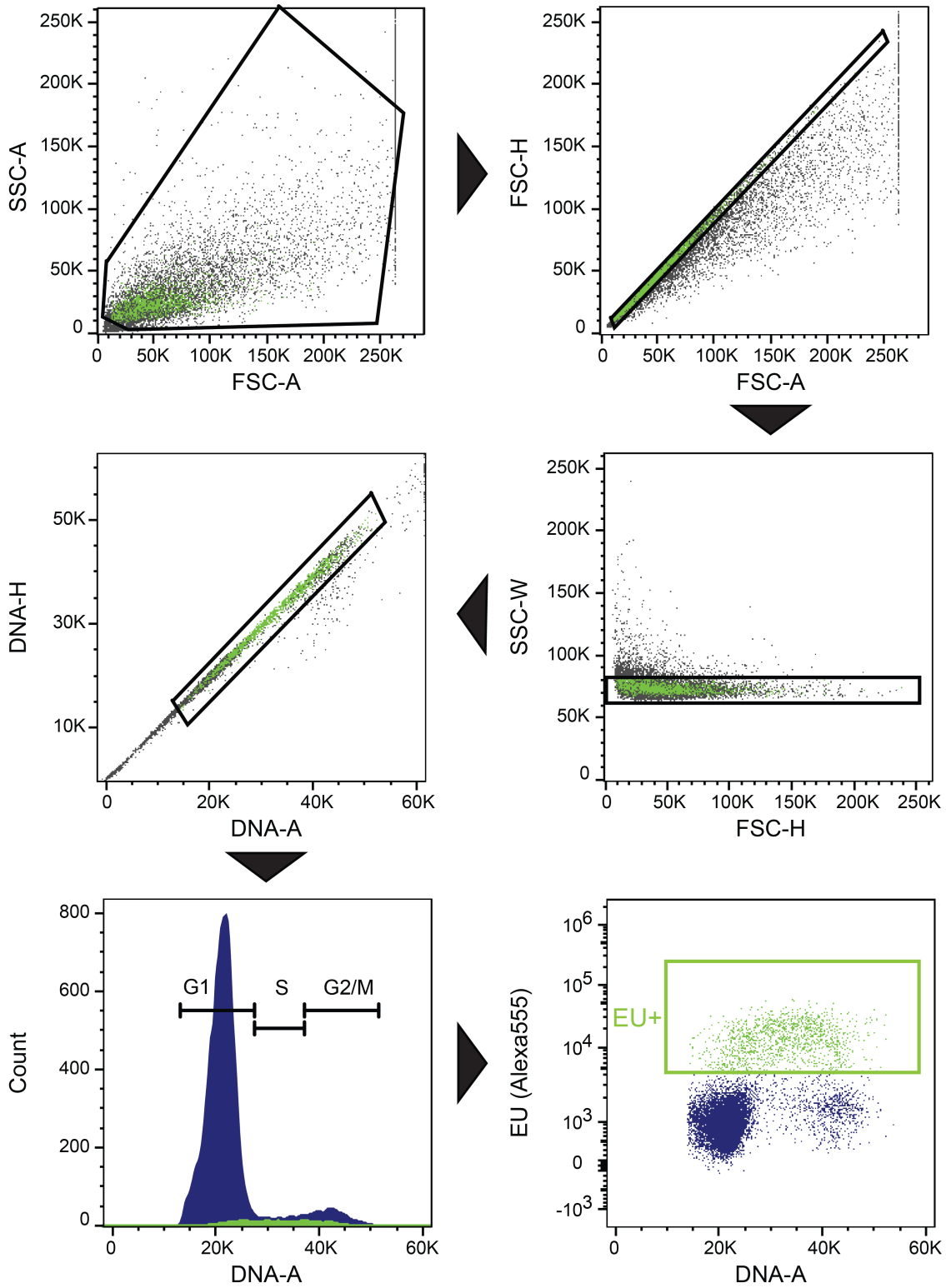

576 **Supplementary Fig. 1. Gating strategy to detect EU signal (Alexa 555) using flow**
577 **cytometry.** For gating cells, very small events were excluded based on size and
578 granularity in the FSC-A/SSC-A gate, followed by gating for linear relation between

579 FSC-A and FSC-H to remove cell aggregates. We limited the analysis to events with
580 low side scattering by gating in FSC-H/SSC-W and plotted the resulting population
581 based on a linear relation in FxCycleViolet dye intensity of area and height (DNA-
582 A/DNA-H) within a range that corresponds to 2N to 4N DNA content. This gate
583 contains cells within the cell cycle and constitutes the base population for the
584 calculation of the EU positive cells. Based on the fluorescence signal of DMSO
585 controls in the DNA-A / Alexa555-A plot, we set a threshold gate above which cells
586 were considered EU positive. EU+ population was backgated and indicated as green
587 overlay in the parental gates.

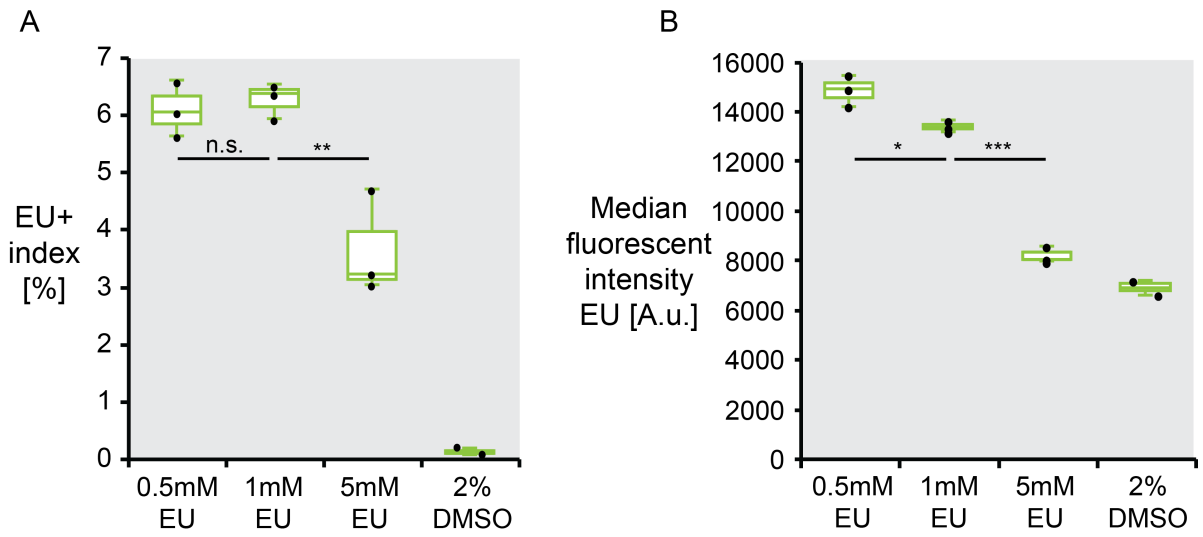

Supplementary Fig. 2. Fraction of EU positive cells and their median fluorescence after 2 hours of labelling with different EU concentrations. Box plots depicting the fraction (A) and the median fluorescent signal intensity (B) of EU+ cells at different concentrations of EU and at 2% DMSO. Box plots indicate median (middle line), 25th, 75th percentile (box) and 5th and 95th percentile (whiskers). Dots show single data points. Differences between concentrations were calculated using One-way ANOVA with Tukey's HSD post hoc test for pairwise comparisons. n.s.: not significant, *: $p > 0.05$, **: $p > 0.01$, ***: $p > 0.001$.

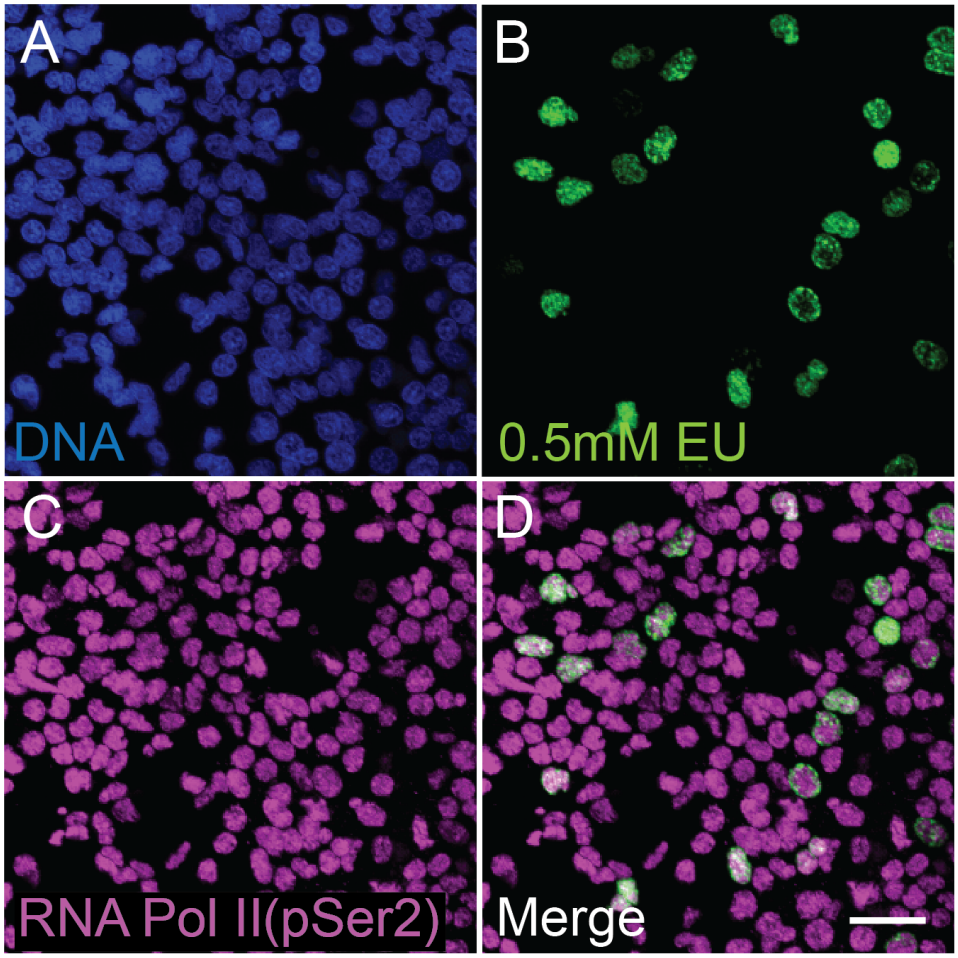

Supplementary Fig. 3. EU labels a small subset of transcriptionally active cells. Confocal imaging stack of epidermal cells shows that EU (B, D; 2h pulse) labels only a fraction of cells detected by an antibody against phospho-Ser2 of the C-terminal domain of RNA polymerase II (C, D). Nuclear stain (blue): Hoechst33342. Scale bar: 10μm.

601 ## References

602 **Akbalik, G., Langebeck-Jensen, K., Tushev, G., Sambandan, S., Rinne, J., Epstein, I.,**
603 **Cajigas, I., Vlatkovic, I. and Schuman, E. M.** (2017). Visualization of newly
604 synthesized neuronal RNA in vitro and in vivo using click-chemistry. *RNA Biol* **14**,
605 20-28.
606 **Alberts, B., Johnson, A., Lewis, J., Morgan, D., Raff, M., Roberts, K. and Walter, P.**
607 (2016). Molecular biology of the cell, 6th edn New York. *NY: Garland Science*.
608 **Amano, M., Leblond, C. P. and Nadler, N. J.** (1965). Radioautographic Analysis of
609 Nuclear Rna in Mouse Cells Revealing Three Pools with Different Turnover Times.
610 *Exp Cell Res* **38**, 314-340.
611 **Amiel, A. R., Johnston, H. T., Nedoncelle, K., Warner, J. F., Ferreira, S. and Rottinger,**
612 **E.** (2015). Characterization of Morphological and Cellular Events Underlying Oral
613 Regeneration in the Sea Anemone, Nematostella vectensis. *Int J Mol Sci* **16**, 28449-
614 28471.
615 **Arendt, D., Musser, J. M., Baker, C. V. H., Bergman, A., Cepko, C., Erwin, D. H.,**
616 **Pavlicev, M., Schlosser, G., Widder, S., Laubichler, M. D., et al.** (2016). The
617 origin and evolution of cell types. *Nat Rev Genet* **17**, 744-757.
618 **Briquet, S., Marinach, C., Silvie, O. and Vaquero, C.** (2020). Preparing for Transmission:
619 Gene Regulation in Plasmodium Sporozoites. *Front Cell Infect Microbiol* **10**, 618430.
620 **Bryant, C. J., McCool, M. A., Abriola, L., Surovtseva, Y. V. and Baserga, S. J.** (2022). A
621 high-throughput assay for directly monitoring nucleolar rRNA biogenesis. *Open Biol*
622 **12**, 210305.
623 **Buzgariu, W., Wenger, Y., Tcaciuc, N., Catunda-Lemos, A. P. and Galliot, B.** (2018).
624 Impact of cycling cells and cell cycle regulation on Hydra regeneration. *Dev Biol* **433**,
625 240-253.
626 **Chalabi-Dchar, M., Fenouil, T., Machon, C., Vincent, A., Catez, F., Marcel, V., Mertani,**
627 **H. C., Saurin, J. C., Bouvet, P., Guitton, J., et al.** (2021). A novel view on an old
628 drug, 5-fluorouracil: an unexpected RNA modifier with intriguing impact on cancer
629 cell fate. *NAR Cancer* **3**, zcab032.
630 **Chen, D., Yan, W., Fu, L. Y. and Kaufmann, K.** (2018). Architecture of gene regulatory
631 networks controlling flower development in Arabidopsis thaliana. *Nat Commun* **9**,
632 4534.
633 **Core, L. J., Waterfall, J. J. and Lis, J. T.** (2008). Nascent RNA sequencing reveals
634 widespread pausing and divergent initiation at human promoters. *Science* **322**, 1845-
635 1848.
636 **Desvergne, B., Michalik, L. and Wahli, W.** (2006). Transcriptional regulation of
637 metabolism. *Physiol Rev* **86**, 465-514.
638 **Dvorackova, M. and Fajkus, J.** (2018). Visualization of the Nucleolus Using Ethynyl
639 Uridine. *Front Plant Sci* **9**, 177.
640 **Febrimarsa, Gornik, S. G., Barreira, S. N., Salinas-Saavedra, M., Schnitzler, C. E.,**
641 **Baxevanis, A. D. and Frank, U.** (2023). Randomly incorporated genomic N6-
642 methyldeoxyadenosine delays zygotic transcription initiation in a cnidarian. *EMBO J*
643 **42**, e112934.
644 **Fritzenwanker, J. H. and Technau, U.** (2002). Induction of gametogenesis in the basal
645 cnidarian *Nematostella vectensis*. *Dev Genes Evol* **212**, 99-103.

Fujisawa, T. and David, C. N. (1982). Commitment during stenotele differentiation in Hydra is localized near the S/G2 boundary in the terminal cell cycle. *Dev Biol* **93**, 226-230.

García-Castro, H., Kenny, N. J., Iglesias, M., Álvarez-Campos, P., Mason, V., Elek, A., Schönauer, A., Sleight, V. A., Neiro, J. and Aboobaker, A. (2021). ACME dissociation: a versatile cell fixation-dissociation method for single-cell transcriptomics. *Genome biology* **22**, 1-34.

Garschall, K., Pascual-Carreras, E., Garcia-Pascual, B., Filimonova, D., Guse, A., Johnston, I. G. and Steinmetz, P. R. (2024). The cellular basis of feeding-dependent body size plasticity in sea anemones. *Development* **151**, dev202926.

Goldberg, I. H., Rabinowitz, M. and Reich, E. (1962). Basis of actinomycin action. I. DNA binding and inhibition of RNA-polymerase synthetic reactions by actinomycin. *Proc Natl Acad Sci U S A* **48**, 2094-2101.

Greene, B. L., Kang, G., Cui, C., Bennati, M., Nocera, D. G., Drennan, C. L. and Stubbe, J. (2020). Ribonucleotide Reductases: Structure, Chemistry, and Metabolism Suggest New Therapeutic Targets. *Annu Rev Biochem* **89**, 45-75.

Hand, C. and Uhlinger, K. R. (1992). The culture, sexual and asexual reproduction, and growth of the sea anemone *Nematostella vectensis*. *Biol Bull* **182**, 169-176.

Hobert, O. (2008). Regulatory logic of neuronal diversity: terminal selector genes and selector motifs. *Proc Natl Acad Sci U S A* **105**, 20067-20071.

Hoffman, E. A., Frey, B. L., Smith, L. M. and Auble, D. T. (2015). Formaldehyde crosslinking: a tool for the study of chromatin complexes. *J Biol Chem* **290**, 26404-26411.

Ierusalimsky, V. N. and Balaban, P. M. (2016). RNA synthesis and turnover in the molluscan nervous system studied by Click-iT method. *Brain Res* **1633**, 139-148.

---- (2018). Long-living RNA in the CNS of terrestrial snail. *RNA Biol* **15**, 207-213.

Jahnel, S. M., Walzl, M. and Technau, U. (2014). Development and epithelial organisation of muscle cells in the sea anemone Nematostella vectensis. *Front Zool* **11**, 44.

Jao, C. Y. and Salic, A. (2008). Exploring RNA transcription and turnover in vivo by using click chemistry. *Proceedings of the National Academy of Sciences* **105**, 15779-15784.

Jordan, A. and Reichard, P. (1998). Ribonucleotide reductases. *Annu Rev Biochem* **67**, 71-98.

Kaufmann, K., Pajoro, A. and Angenent, G. C. (2010). Regulation of transcription in plants: mechanisms controlling developmental switches. *Nat Rev Genet* **11**, 830-842.

Kedinger, C., Gniazdowski, M., Mandel, J. L., Jr., Gissinger, F. and Chambon, P. (1970). Alpha-amanitin: a specific inhibitor of one of two DNA-pendent RNA polymerase activities from calf thymus. *Biochem Biophys Res Commun* **38**, 165-171.

Konrad, C. G. (1963). Protein Synthesis and Rna Synthesis during Mitosis in Animal Cells. *J Cell Biol* **19**, 267-277.

Levine, M. (2010). Transcriptional enhancers in animal development and evolution. *Curr Biol* **20**, R754-763.

Lindell, T. J., Weinberg, F., Morris, P. W., Roeder, R. G. and Rutter, W. J. (1970). Specific inhibition of nuclear RNA polymerase II by alpha-amanitin. *Science* **170**, 447-449.

Long, M. J., Ly, P. and Aye, Y. (2022). Still no Rest for the Reductases: Ribonucleotide Reductase (RNR) Structure and Function: An Update. *Macromolecular Protein Complexes IV: Structure and Function*, 155-197.

Longley, D. B., Harkin, D. P. and Johnston, P. G. (2003). 5-fluorouracil: mechanisms of action and clinical strategies. *Nat Rev Cancer* **3**, 330-338.

695 **Major, P., Egan, E., Herrick, D. and Kufe, D.** (1982). 5-Fluorouracil incorporation in DNA
696 of human breast carcinoma cells. *Cancer research* **42**, 3005-3009.
697 **Mazo, G.** (2021). QuickFigures: A toolkit and ImageJ PlugIn to quickly transform
698 microscope images into scientific figures. *PLoS One* **16**, e0240280.
699 **Messikommer, A., Seipel, K., Byrne, S., Valk, P. J. M., Pabst, T. and Luedtke, N. W.**
700 (2020). RNA Targeting in Acute Myeloid Leukemia. *ACS Pharmacol Transl Sci* **3**,
701 1225-1232.
702 **Mikhaleva, E. A., Leinsoo, T. A., Ishizu, H., Gvozdev, V. A. and Klenov, M. S.** (2019).
703 The nucleolar transcriptome regulates Piwi shuttling between the nucleolus and the
704 nucleoplasm. *Chromosome Research* **27**, 141-152.
705 **Nainar, S., Cuthbert, B. J., Lim, N. M., England, W. E., Ke, K., Sophal, K., Quechol, R.,**
706 **Mobley, D. L., Goulding, C. W. and Spitale, R. C.** (2020). An optimized chemical-
707 genetic method for cell-specific metabolic labeling of RNA. *Nat Methods* **17**, 311-
708 318.
709 **Naro, C., Jolly, A., Di Persio, S., Bielli, P., Setterblad, N., Alberdi, A. J., Vicini, E.,**
710 **Geremia, R., De la Grange, P. and Sette, C.** (2017). An Orchestrated Intron
711 Retention Program in Meiosis Controls Timely Usage of Transcripts during Germ
712 Cell Differentiation. *Dev Cell* **41**, 82-93 e84.
713 **Nordlund, P. and Reichard, P.** (2006). Ribonucleotide reductases. *Annu Rev Biochem* **75**,
714 681-706.
715 **Perry, R. P.** (1962). The Cellular Sites of Synthesis of Ribosomal and 4s Rna. *Proc Natl*
716 *Acad Sci U S A* **48**, 2179-2186.
717 **Qu, D., Zhou, L., Wang, W., Wang, Z., Wang, G., Chi, W. and Zhang, B.** (2013). 5-
718 Ethynylcytidine as a new agent for detecting RNA synthesis in live cells by "click"
719 chemistry. *Anal Biochem* **434**, 128-135.
720 **Rabani, M., Levin, J. Z., Fan, L., Adiconis, X., Raychowdhury, R., Garber, M., Gnirke,**
721 **A., Nusbaum, C., Hacohen, N., Friedman, N., et al.** (2011). Metabolic labeling of
722 RNA uncovers principles of RNA production and degradation dynamics in
723 mammalian cells. *Nat Biotechnol* **29**, 436-442.
724 **Radle, B., Rutkowski, A. J., Ruzsics, Z., Friedel, C. C., Koszinowski, U. H. and Dolken,**
725 **L.** (2013). Metabolic labeling of newly transcribed RNA for high resolution gene
726 expression profiling of RNA synthesis, processing and decay in cell culture. *J Vis*
727 *Exp*.
728 **Scherrer, K. and Darnell, J. E.** (1962). Sedimentation characteristics of rapidly labelled
729 RNA from HeLa cells. *Biochem Biophys Res Commun* **7**, 486-490.
730 **Schindelin, J., Arganda-Carreras, I., Frise, E., Kaynig, V., Longair, M., Pietzsch, T.,**
731 **Preibisch, S., Rueden, C., Saalfeld, S., Schmid, B., et al.** (2012). Fiji: an open-
732 source platform for biological-image analysis. *Nat Methods* **9**, 676-682.
733 **Schindelin, J., Rueden, C. T., Hiner, M. C. and Eliceiri, K. W.** (2015). The ImageJ
734 ecosystem: An open platform for biomedical image analysis. *Molecular reproduction*
735 *and development* **82**, 518-529.
736 **Sharma, R. C., Murphy, A. J., DeWald, M. G. and Schimke, R. T.** (1993). A rapid
737 procedure for isolation of RNA-free genomic DNA from mammalian cells.
738 *Biotechniques* **14**, 176-178.
739 **Skoog, L. and Nordenskjold, B.** (1971). Effects of hydroxyurea and 1-beta-D-
740 arabinofuranosyl-cytosine on deoxyribonucleotide pools in mouse embryo cells. *Eur J*
741 *Biochem* **19**, 81-89.
742 **Slater, M. L.** (1973). Effect of reversible inhibition of deoxyribonucleic acid synthesis on the
743 yeast cell cycle. *J Bacteriol* **113**, 263-270.

Sobell, H. M. (1985). Actinomycin and DNA transcription. *Proc Natl Acad Sci U S A* **82**, 5328-5331.

Spriggs, D., Robbins, G., Mitchell, T. and Kufe, D. (1986). Incorporation of 9-beta-D-arabinofuranosyl-2-fluoroadenine into HL-60 cellular RNA and DNA. *Biochem Pharmacol* **35**, 247-252.

Stein, H. and Hausen, P. (1969). Enzyme from calf thymus degrading the RNA moiety of DNA-RNA Hybrids: effect on DNA-dependent RNA polymerase. *Science* **166**, 393-395.

Tkatchenko, A. V. (2006). Whole-mount BrdU staining of proliferating cells by DNase treatment: application to postnatal mammalian retina. *Biotechniques* **40**, 29-30, 32.

Uddin, M., Altmann, G. and Leblond, C. (1984). Radioautographic visualization of differences in the pattern of [3H] uridine and [3H] orotic acid incorporation into the RNA of migrating columnar cells in the rat small intestine. *The Journal of cell biology* **98**, 1619-1629.

Van't Sant, L. J., White, J. J., Hoeijmakers, J. H. J., Vermeij, W. P. and Jaarsma, D. (2021). In vivo 5-ethynyluridine (EU) labelling detects reduced transcription in Purkinje cell degeneration mouse mutants, but can itself induce neurodegeneration. *Acta Neuropathol Commun* **9**, 94.

Voet, D., Voet, J. G. and Pratt, C. W. (2016). *Fundamentals of biochemistry: life at the molecular level*: John Wiley & Sons.

Wang, J., Rojas, P., Mao, J., Muste Sadurni, M., Garnier, O., Xiao, S., Higgs, M. R., Garcia, P. and Saponaro, M. (2021). Persistence of RNA transcription during DNA replication delays duplication of transcription start sites until G2/M. *Cell Rep* **34**, 108759.

Zhang, W., Zhang, M., Ma, L., Jariyasakulroj, S., Chang, Q., Lin, Z., Lu, Z. and Chen, J. F. (2024). Recapitulating and reversing human brain ribosomopathy defects via the maladaptive integrated stress response. *Sci Adv* **10**, eadk1034.

Zocher, S., McCloskey, A., Karasinsky, A., Schulte, R., Friedrich, U., Lesche, M., Rund, N., Gage, F. H., Hetzer, M. W. and Toda, T. (2024). Lifelong persistence of nuclear RNAs in the mouse brain. *Science* **384**, 53-59.